Infrared Lattice Vibrations and Free-Electron Dispersion in GaN

A. S. Barker, Jr. and M. Ilegems
Bell Laboratories, Murray Hill, New Jersey 07974
(Received 28 July 1972)

Infrared reflectivity and absorption measurements have been made on single-crystal epitaxial GaN on (0001) α-Al_2O_3 crystals. Analysis of the normal-incidence reflectance data on low-carrier-concentration layers using the Kramers–Kronig technique and dielectric oscillator fits yields the values $\omega_{TO}^{\perp}=560$ cm^{-1} and $\omega_{LO}^{\perp}=746$ cm^{-1} for the optical mode frequencies at 300 K. Adopting $\epsilon_{\infty}^{\perp}=5.35$ from a fit to Ejder's refractive-index data the additional quantities $\epsilon_{o}^{\perp}=9.5$ for the static dielectric constant, $e_B^{*\perp}=2.65e$ for the Born effective charge, and $\alpha^{\perp}=0.44$ for the polaron coupling constant are derived. Reflectivity measurements at 50° incidence with s and p polarizations show that the longitudinal lattice mode is nearly isotropic. Using the value $\omega_{TO}^{\parallel}=533$ cm^{-1} from Raman data the values $\omega_{LO}^{\parallel}=744$ cm^{-1}, $\epsilon_{o}^{\parallel}=10.4$, $e_B^{*\parallel}=2.82e$, and $\alpha^{\parallel}=0.49$ are obtained from oscillator fits to the 50° incidence data. Information on the free-carrier effects in GaN was obtained by studying the normal-incidence reflectance as a function of carrier concentration in the 2×10^{17} to 1×10^{20} cm^{-3} range. By fitting the reflectance minima versus concentration data, a value of $m^*/m=(0.20\pm0.02)$ for the optical effective mass is obtained. Measurements at 50° incidence show that the plasma frequency is isotropic within experimental precision.

I. INTRODUCTION

Gallium nitride is a III-V compound semiconductor which crystallizes in the wurtzite structure. Much recent work has concentrated on the optical properties[1] of this compound in the near-gap region, and on stimulated emission[2] and luminescence.[3] An early study[4] of the infrared spectrum of small needles of GaN allowed estimates to be made of the bare lattice dielectric dispersion due to optical lattice modes. The present work (made possible by the availability of larger crystals of GaN), presents a much more complete study of the lattice dispersion. By studying a series of samples extending in carrier concentration from ~ 10^{17} to ~ 10^{20} electrons/cm^3, and by separating the intrinsic lattice dispersion and free-carrier dispersion, information on both the carriers and the lattice vibrations has been obtained. Section II presents the experimental details. In Sec. III the bound-electron contribution to the infrared dispersion is evaluated. Using this information we analyze the intrinsic lattice dispersion in Sec. IV and the free-electron mass and damping in Sec. V.

II. SAMPLE PREPARATION AND EXPERIMENTAL METHODS

The GaN crystals used in this study were grown as epitaxial layers on (0001)-oriented sapphire substrates.[5] The layers had thicknesses ranging from 5 to 100 μm. Figure 1 shows the sample orientation. Details of the growth procedure and electrical characteristics of these layers are described elsewhere.[5,6] The samples were prepared for the infrared experiments by polishing a flat surface using 1-μm diamond paste on a tin lap. A few samples had quite smooth as-grown surfaces and could be measured without the polishing treatment. Reflectivity measurements were made in the 1–35-μm region at room temperature using the prism spectrometer and techniques described by Spitzer and Kleinman.[7] No polarizer is necessary for these near-normal-incidence measurements since for all rays the electric vector E is approximately normal to the wurtzite c axis for the samples shown in Fig. 1. As described below some measurements were made with an angle of incidence of 50 degrees to obtain information on the $\vec{E}\parallel\vec{c}$ axis (extraordinary ray) optical properties. For these measurements a polarizer is used to obtain R_p ($\vec{E}$ parallel to the plane of incidence) and R_s ($\vec{E}$ perpendicular to the plane of incidence) spectra. The reflection spectra were analyzed by Kramers–Kronig integral transforms and oscillator fits using

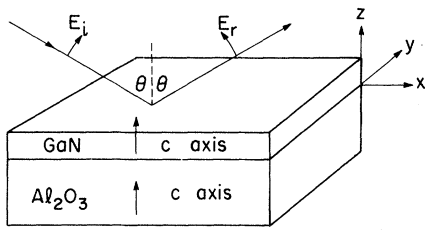

$$\epsilon=\begin{pmatrix}\epsilon^{xx}(\omega) & 0 & 0\\ 0 & \epsilon^{yy}(\omega) & 0\\ 0 & 0 & \epsilon^{zz}(\omega)\end{pmatrix}$$

$$\epsilon^{xx}=\epsilon^{yy}=\epsilon^{\perp}\quad;\quad\epsilon^{zz}=\epsilon^{\parallel}$$

FIG. 1. Growth habit of the GaN samples used in the present study. The upper part of the sketch shows the beam geometry and polarization used to measure R_p. The lower part of the figure shows the two independent tensor components needed to describe the dielectric dispersion.

methods which have been described in earlier papers.[7,8] Some room-temperature transmission measurements were made at normal incidence. After corrections for reflectivity and for loss in the sapphire substrate, these data are reduced to absorption coefficient α using the equation

$$I/I_0 = e^{-\alpha t} ,$$

where I_0 is the beam power entering the GaN, I the power leaving the far side, and t the sample thickness in cm. Since some of the GaN layers had a graded thickness care was taken to measure the thickness and Hall coefficient in the actual region used for the optical experiments.

III. BOUND-ELECTRON DISPERSION

In order to fit accurately the lattice dispersion and free-carrier dispersion in the infrared frequency region it is necessary to know the dielectric constant ϵ_∞ due to all higher-lying transitions. Manchon *et al.*[4] made a rough estimate of $\epsilon_\infty = 5.8$ for the electric vector $\vec{E}$ both parallel and perpendicular to the $\vec{c}$ axis using the apparent thickness method on very small samples. In what follows the superscripts $\perp$ and $\parallel$ will be used to distinguish the ordinary and extraordinary optical properties. We have recently redetermined $\epsilon_\infty^\perp(\vec{E}\perp\vec{c})$ by ellipsometry to be $5.42 \pm 3\%$ at $\lambda = 5460$ Å, which suggests that the earlier value was too large. Ejder[9] has published index data in the range 1–3.4 eV which now appear to be the best data available. We have fit Ejder's data and find that they are adequately described in the 1–3.4 eV range by the expression

$$\epsilon^\perp = 3.6 + \frac{1.75}{1-(\hbar\omega/4.85)^2} , \qquad (1)$$

with $\hbar\omega$ given in eV. In the infrared frequency range well below 1 eV the electronic dispersion described by Eq. (1) becomes flat with the value

$$\epsilon_\infty^\perp = 5.35 . \qquad (2)$$

The uncertainty in Ejder's measurement suggests that Eq. (2) is accurate to better than 4%.

IV. INFRARED-ACTIVE LATTICE VIBRATIONS

A. Modes for $\vec{E}\perp\vec{c}$ Axis

The principal hindrances to obtaining accurate infrared phonon data in the early work on GaN were small sample size and the highly conducting (n-type) nature of the crystals.[4] The epitaxial samples produced for the present work were of sufficiently large area and low carrier concentration to overcome both of these problems. To obtain the intrinsic lattice reflectivity two approaches were followed. In the first approach, a sample was bombarded by 1-MeV electrons to reduce the carrier concentration below 10^{18} electrons/cm^{-3}. Reflection spectra were then measured in the wavelength range 1–35 μm. The analysis of this data is discussed below. The second approach consisted of measuring the reflectivity and the Hall coefficient for a series of layers having carrier concentrations ranging from $\sim 2\times 10^{17}$ cm^{-3} to $\sim 1\times 10^{20}$ cm^{-3}. The effect of the carriers can then be subtracted out by simultaneously and accurately fitting both the lattice and carrier effects. Since this method gave the same result as the first method for the properties of the insulating lattice we reserve discussion of these fits for the section on carrier effects. Figure 2(a) shows the measured reflection spectrum of GaN after 240 m μA h of bombardment by 1-MeV electrons. (Identical spectra were obtained without bombardment on an as-grown layer with a carrier concentration of $n = 2\times 10^{17}$ cm^{-3}.) The remnant conductivity is very inhomogeneous; however, Hall measurements show that the sample is n type with electron concentration below 10^{18} cm^{-3}. A Kramers–Kronig analysis[7,8] of the data in Fig. 2(a) yields all the optical constants for the sample. We shall be most concerned with the dielectric function $\epsilon(\omega)$. In Fig. 2(b) we have plotted $\mathrm{Im}(\epsilon^\perp)$ to show the transverse-mode structure and $\mathrm{Im}(-1/\epsilon^\perp)$ for the longitudinal-mode structure. One mode of each type is observed, as is expected for an insulating wurtzite-type crystal. The mode frequencies are given in Table I. Figure 2(c) shows the result of a Kramers–Kronig analysis of a reflectivity spectrum taken earlier when the sample had received only half the bombardment treatment. $\mathrm{Im}(\epsilon^\perp)$ clearly shows free-carrier absorption with the superimposed transverse lattice mode at 560 cm^{-1}. The $\mathrm{Im}(-1/\epsilon^\perp)$ spectrum shows two peaks,

TABLE I. Infrared dielectric properties of GaN for $\vec{E}\perp\vec{c}$ axis with free carriers removed by electron bombardment.

$\epsilon_\infty^\perp = 5.35$	Index fit
$\omega_{TO}^\perp = 560$ cm$^{-1}\pm 1\%$	Kramers–Kronig analysis
$\omega_{LO}^\perp = 746$ cm$^{-1}\pm 1\%$	Kramers–Kronig analysis
$\omega_0^\perp = 560$ cm$^{-1}\pm 1\%$	Reflectivity fit [see Eq. (3)]
$S^\perp = 4.1 \pm 2\%$	Reflectivity fit [see Eq. (3)]
$\Gamma^\perp = 17$ cm$^{-1}\pm 20\%$	Reflectivity fit [see Eq. (3)]
Derived Quantities	
$\epsilon_0^\perp = 9.5 \pm 3\%$	Low-frequency dielectric constant
$e_B^{*\perp}/e = 2.65 \pm 2\%$	Born lattice charge
$\alpha^\perp = 0.44 \pm 2\%$	Polaron coupling constant (assuming $m^*/m = 0.2$)

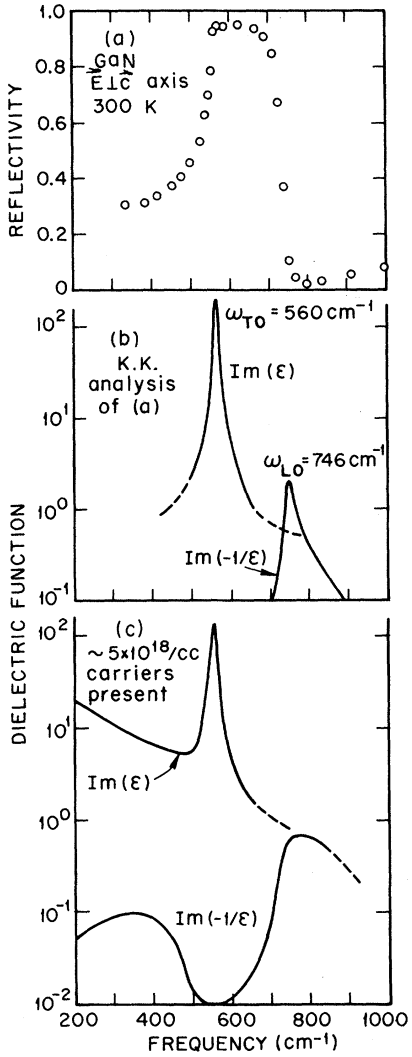

FIG. 2. (a) Reflectivity of GaN after 240 μA h of 1-MeV electron bombardment to remove free carriers. (b) Dielectric functions derived from reflectivity by Kramers–Kronig analysis. (c) Dielectric functions derived from the reflectivity at an earlier stage when the irradiation was only half completed. Note the shifted LO mode near 760 cm^{-1} and the extra LO mode at 350 cm^{-1} compared with Fig. 1(b).

one principally plasmon like at 350 cm^{-1} and the mixed longitudinal-optic (LO) phonon-plasmon at 780 cm^{-1}. It was the appearance of the 350 cm^{-1} plasmon peak as well as conductivity measurements which showed that more bombardment was needed to produce a pure lattice spectrum.

In addition to the Kramers–Kronig analysis [Fig. 2(b)], several trial fits were made to the reflectivity spectrum in Fig. 2(a). For this purpose the simple three-parameter form

$$\epsilon^{\perp} = 5.35 + \frac{S^{\perp}(\omega_0^{\perp})^2}{(\omega_0^{\perp})^2 - \omega^2 - i\omega\Gamma^{\perp}} \tag{3}$$

was assumed for the dielectric function. $S^{\perp}$ is the mode strength, $\omega_0^{\perp}$ the mode frequency, and $\Gamma^{\perp}$ the mode linewidth. Fits to reflectivity spectra using such functions have been described extensively in the literature.[7,8] The best fit was obtained with $\omega_0^{\perp} = 560$ cm^{-1} in agreement with $\omega_{TO}^{\perp}$ obtained from the Kramers–Kronig analysis. The LO mode frequency (ω_{LO}) may be obtained by finding the zero of ϵ in Eq. (3).[8] The result for $\omega_{LO}^{\perp}$ is in good agreement with the 91.5-meV (738 cm^{-1}) LO-phonon interval observed at 4.2 K in luminescence.[10] The remaining parameters are given in Table I. Finally we may derive several properties of the infrared-active lattice vibrations using the data obtained thus far. These are the low-frequency dielectric constant $\epsilon_0^{\perp}$, the Born lattice-dynamic charge[11] $e_B^{*\perp}$, and the Fröhlich electron-phonon coupling constant[12] $\alpha^{\perp}$. For $\alpha^{\perp}$ we have used the effective mass discussed in Sec. V. The values of $\epsilon_0^{\perp}$ and $e_B^{*\perp}$ (Table I) are smaller than the rough estimates presented earlier[4]; however, the general conclusion that GaN is much more ionic than many other III-V compounds is still valid. A discussion of the ionicity of GaN has been presented in the earlier work.[4]

B. Modes for $\vec{E} \| \vec{c}$ Axis

Figure 1 shows the orientation of the samples used in the present study. The wurtzite c axis is perpendicular to the plane face. For a wurtzite crystal the dielectric function is a tensor as shown in the lower part of the figure. The reflection data which give the parameters in Table I are obtained near normal incidence ($\theta = 0$ in Fig. 1). For such a geometry the Fresnel formula for the reflectivity is

$$R(\theta = 0) = \left| \frac{1 - (1/\epsilon^{xx})^{1/2}}{1 + (1/\epsilon^{xx})^{1/2}} \right|^2 , \tag{4}$$

so that only one component of the dielectric tensor ϵ^{xx} can be measured.[13] If we consider non-normal incidence with the infrared beam polarized in the plane of incidence, the Fresnel formula becomes

$$R_p = \left| \frac{\cos\theta - [(\epsilon^{zz} - \sin^2\theta)/\epsilon^{zz}\epsilon^{xx}]^{1/2}}{\cos\theta + [(\epsilon^{zz} - \sin^2\theta)/\epsilon^{zz}\epsilon^{xx}]^{1/2}} \right|^2 . \tag{5}$$

For the beam polarized perpendicular to the plane of incidence the reflectivity is

$$R_s = \left| \frac{\cos\theta - (\epsilon^{yy} - \sin^2\theta)^{1/2}}{\cos\theta + (\epsilon^{yy} - \sin^2\theta)^{1/2}} \right|^2 , \tag{6}$$

where $\epsilon^{yy} = \epsilon^{xx} \equiv \epsilon^{\perp}$ for the wurtzite crystal[12] shown in Fig. 1. From Eq. (5) it can be seen that R_p contains information on both ϵ^{xx} and ϵ^{zz}. On closer examination we note that the ϵ^{zz} dependence cancels out near the pole of ϵ^{zz}, so we cannot find the pole or ω_{TO} optic mode for vibrations along the c axis. R_p is very sensitive, however, to the zero in ϵ^{zz}

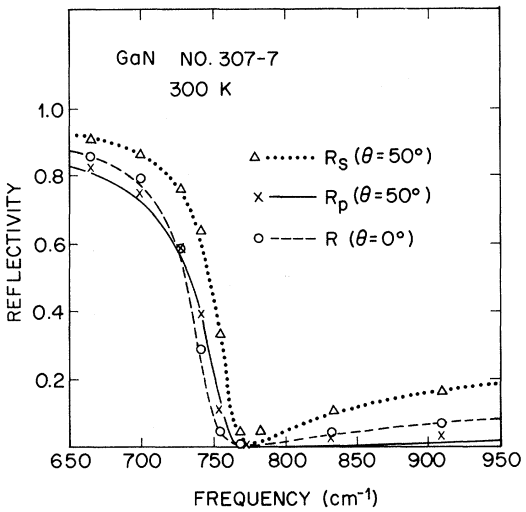

FIG. 3. Measurement of a s-polarized and p-polarized reflectivity for $\theta = 50°$. Good fits are obtained by assuming that the dielectric functions $\epsilon^{\perp}$ and $\epsilon^{\parallel}$ are equal near 750 cm^{-1}; i.e., that the LO mode is isotropic.

and we now exploit this fact.

Figure 3 shows R_p measured for a sample at $\theta = 50°$ for two polarizations. In addition the normal-incidence spectrum is also shown for comparison. The curves are fits using Eqs. (4)–(6) and the dielectric functions

$$\epsilon^{xx} \equiv \epsilon^{\perp} = \epsilon_{\infty}^{\perp} + \frac{S^{\perp}(\omega_0^{\perp})^2}{(\omega_0^{\perp})^2 - \omega^2 - i\omega\Gamma^{\perp}}, \tag{7}$$

$$\epsilon^{zz} \equiv \epsilon^{\parallel} = \epsilon_{\infty}^{\parallel} + \frac{S^{\parallel}(\omega_0^{\parallel})^2}{(\omega_0^{\parallel})^2 - \omega^2 - i\omega\Gamma^{\parallel}}, \tag{8}$$

where the parameters $\epsilon_{\infty}^{\perp}$, $S^{\perp}$, $\omega_0^{\perp}$, and $\Gamma^{\perp}$ have already been determined (Table I). For the reason explained above we find that R_p is not sensitive to $\omega_0^{\parallel}$ but is very sensitive to the combination of parameters $\omega_0^{\parallel}(1 + S^{\parallel}/\epsilon_{\infty}^{\parallel})^{1/2}$ which determine the zero of $\epsilon^{\parallel}$ (i.e., the LO mode). If we adopt the value $\omega_0^{\parallel}$ from Ref. 4, and assume ϵ_{∞} is isotropic,[4] the fits in Fig. 3 allow the complete evaluation of the dielectric properties as shown in Table II. The fits have been adjusted to best reproduce the steep edge, which is the experimental feature that is most parameter sensitive. The fit to the absolute value of R away from the edge has been judged satisfactory considering the quality of the sample surface. The fits show that the anisotropy of ω_{LO} in GaN is very small, being less than the experimental uncertainty involved in the measurement of the reflectivity edges near 740 cm^{-1}, i.e., less than 5 cm^{-1}. This is to be contrasted with the 27-cm^{-1} anisotropy of the transverse-phonon frequency. The anisotropy behavior is similar to that observed in the II-VI wurtzite crystals CdS[14,15] and CdSe.[15] Using the best-fit values of Γ'', $S^{\parallel}$ we are able to evaluate the additional dielectric parameters for $\vec{E} \parallel \vec{c}$ axis as was done for $\vec{E} \perp \vec{c}$ axis (see Table II).

Finally to show the utility and sensitivity of the above method of measuring R_p, we present several plots to simulate the effect of nonisotropic lattice frequencies on the spectra. Figure 4 shows the complete *reststrahlen* band for $\theta = 50°$ for a case where both ω_0 and ω_{LO} modes are nonisotropic.

TABLE II. Infrared dielectric properties of GaN for $\vec{E} \parallel \vec{c}$ axis.

$\epsilon_{\infty}^{\parallel} = 5.35$	Assuming ϵ_{∞} isotropic (see Ref. 4)
$\omega_0^{\parallel} = 533$ cm^{-1}	Raman spectroscopy (Ref. 4)
$S^{\parallel} = 5.08 \pm 4\%$	Reflectivity fit to $R_p(\theta = 50°)$
$\Gamma^{\parallel} = 17$ cm$^{-1} \pm 20\%$	
$\omega_{LO}^{\parallel} = 744$ cm$^{-1} \pm 1\%$	
Derived Quantities	
$\epsilon_0^{\parallel} = 10.4 \pm 3\%$	
$e_B^{*\parallel}/e = 2.82 \pm 2\%$	
$\alpha^{\parallel} = 0.49 \pm 2\%$	(Assuming $m^*/m = 0.2$)

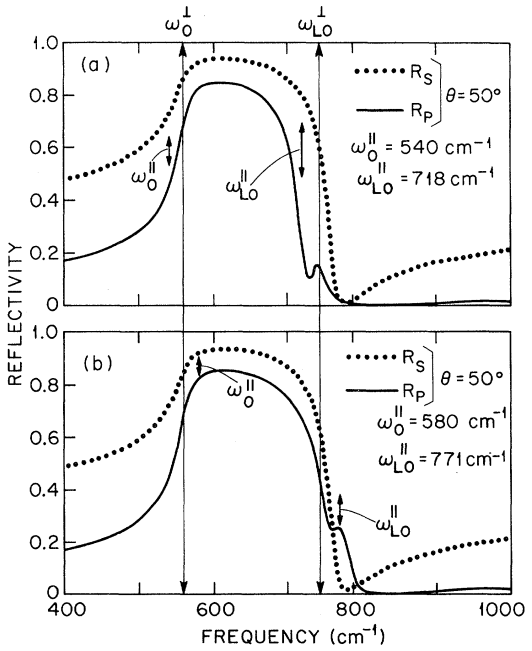

FIG. 4. Calculated reflectivities at $\theta = 50°$ for a uniaxial crystal as shown in Fig. 1 with anisotropic lattice modes. $\epsilon^{\perp}$ is taken to be the same as GaN (see Table I) and the mode frequencies are marked by vertical lines. In (a) $\epsilon^{\parallel}$ has its TO and LO modes at lower frequency and in (b) at higher frequency. The frequency parameters are given in the figure and $\Gamma^{\parallel} = 17$ cm^{-1}. Note that the anisotropy in ω_{LO} is easily distinguished in the R_p spectrum.

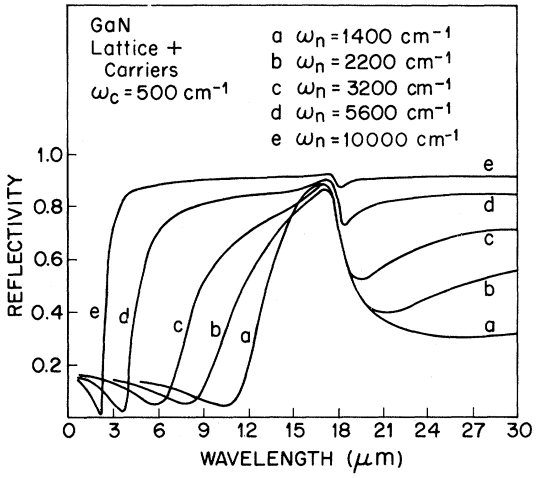

FIG. 5. Calculated reflectivity at normal incidence of GaN with carriers. The carriers are described by the collision frequency ω_c and the density parameter ω_n.

Note that the low-frequency edge of the band remains pinned near $\omega_0^{\perp}$ regardless of $\omega_0^{\parallel}$. The high-frequency edge however is very sensitive to the anisotropy, showing a subsidiary peak for the cases chosen. This peaked structure allows an accurate determination of both $\omega_{LO}^{\perp}$ and $\omega_{LO}^{\parallel}$ directly from the R_p spectrum. We conclude that this reflection technique is very useful for anisotropic crystals which can be prepared with only one plane suitable for optical spectroscopy.

V. FREE-CARRIER ABSORPTION IN GaN

All of the GaN samples studied were n type, many having carrier concentrations in the 10^{19}-cm^{-3} range. As a guide to the reflectance behavior to be expected for such samples we may calculate the optical properties using the dielectric function

$$\epsilon = \epsilon_\infty + \frac{S\omega_0^2}{\omega_0^2 - \omega^2 - i\omega\Gamma} + \frac{\omega_n^2}{-\omega^2 - i\omega\omega_c}, \qquad (9)$$

where[11]

$$\omega_n^2 = 4\pi ne^2/m^* . \qquad (10)$$

The second term in Eq. (9) describes the lattice vibrations as before and the third term describes the free carriers. n is the carrier concentration, m^* the effective mass, and ω_c is the carrier collision frequency. All parameters must have the superscripts $\parallel$ or $\perp$ depending on whether $\vec{E}$ lies along the $\vec{c}$ axis or perpendicular to the $\vec{c}$ axis. Figure 5 shows the normal-incidence reflectivity given by Eq. (9) for a range of ω_n from 1400 to 10^4 cm^{-1}. A value of ω_c = 500 cm^{-1} has been chosen for the carrier damping by using an estimate based on a measured dc mobility of GaN[6] of 80 cm^2/V sec for $n \sim 10^{19}$ cm^{-3}. Figure 5 shows the high-frequency edge of the *reststrahlen* band shifting to higher frequencies as ω_n is increased. In a preliminary study of several GaN samples, behavior like that illustrated in Fig. 5 was observed. Figure 6 shows the reflectivity of sample 307-5 measured out to 16 μm. Two effects were apparent which interfered with exact fits using Eq. (9). First, the reflecting plane of most samples was not smooth, so that the reflectivity was lower than shown in Fig. 5. Since the position of the reflectivity minimum appeared to be independent of surface roughness it was decided to use this feature as a fitting parameter. Second, some samples showed an extra minimum near 12-μm wavelength even though they had large carrier concentrations. Figure 6 illustrates this effect for sample 305-4α. The extraneous minimum near 12 μm is probably connected with inhomogeneities. We observe that if the reflectivity of Fig. 2(a) is averaged with curve e of Fig. 5, a minimum is produced near 12 μm. Samples which showed such subsidiary minima in reflectivity were not included in the analysis.

Figure 7 shows the result of analyzing the reflectivity spectrum and making Hall measurements on 14 samples. There is a good correlation between the frequency of the upper reflectivity minimum and the carrier concentration. Concentration values are estimated accurate within ± 10%, the errors resulting mainly from the uncertainty in the thickness determination for layers that were slightly graded as-grown or after polishing. For some of the larger samples the low-frequency reflectance minimum was also measured and plotted. We next calculated the position of R_{min} using Eq. (9) and various values of ω_n. The position of R_{min} is not very sensitive to the second parameter ω_c; how-

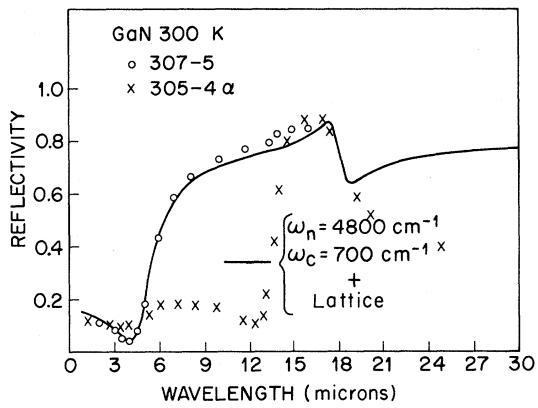

FIG. 6. Reflectivity of conducting samples of GaN. The solid curve is a fit to sample 307-5 using one lattice oscillator (Table I) plus a plasma term. This sample was only large enough to allow measurements out to 16 μm. The two plasma parameters are given in the figure. Sample 305-4α showed an extra minimum near 12 μm, probably due to inhomogenities (see text).

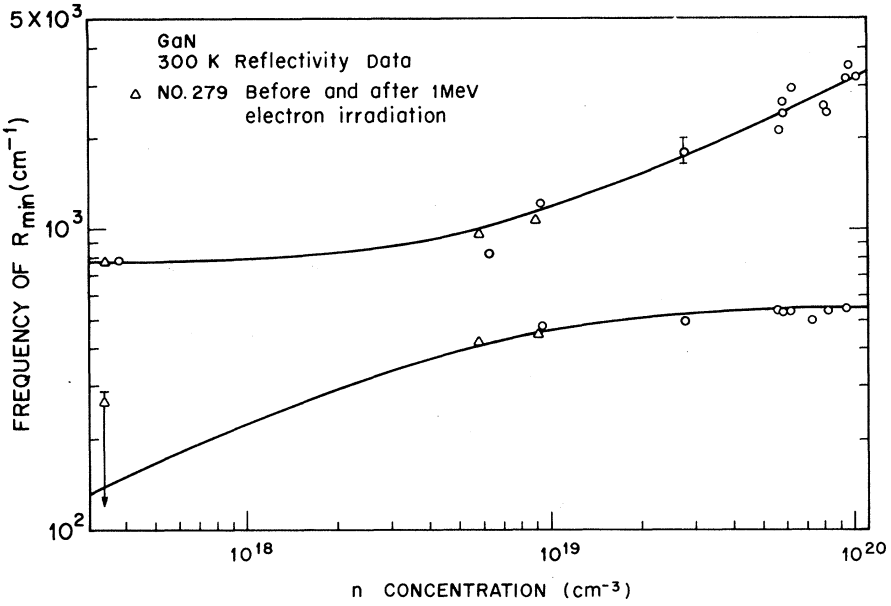

FIG. 7. Frequency of reflectivity minima plotted against concentration. The reflectance is measured at normal incidence ($\vec{E} \perp \vec{c}$ axis). The triangle points were obtained from sample 279 before and after two successive stages of 120 μA h of electron bombardment. The n values for 279 as-grown and after the first bombardment are estimated from resistivity. The lowest frequency triangle represents an upper limit since the minimum had not been encountered at the lowest frequency measurement.

ever, the shape of most of the spectra near R_{min} requires $\omega_c = 600 \pm 100$ cm^{-1} independent of concentration. A graph of the frequency of R_{min} vs $\log\omega_n^2$ can be superimposed on Fig. 7 and adjusted horizontally to give a best fit to the points. The solid curve in Fig. 7 shows this best fit. The fit corresponds to choosing

$$m^*/m = 0.2 . \quad (11)$$

The effective-mass value determined here is somewhat lower than a previous estimate of $m^* = 0.25$ m deduced from luminescence studies.[16] The spread in the measured data points suggests that Eq. (11) has an uncertainty of ± 10%.

Finally, as an independent check on the value of m^* derived above we have made free-carrier absorption measurements by recording the transmittance of several samples. Figure 8(a) shows the absorption coefficient in the range 1.5–4.5-μm wavelength. In this range, for the concentrations studied the approximate relation

$$\alpha \simeq \omega_n^2 \omega_c / c\omega^2 (\epsilon_\infty)^{1/2} , \quad (12)$$

where c is the velocity of light, may be derived from Eq. (9).

TABLE III. Free-carrier dispersion parameters in GaN.

$m^{*\perp} = 0.2$ m ± 10%
$\omega_c^{\perp} = 600$ cm^{-1} ± 15% ($\tau = 0.9 \times 10^{-14}$ sec)
$m^{*\parallel} \simeq m^{*\perp}$ to within 30%
$\omega_c^{\parallel} \simeq \omega_c^{\perp}$ to within 40%

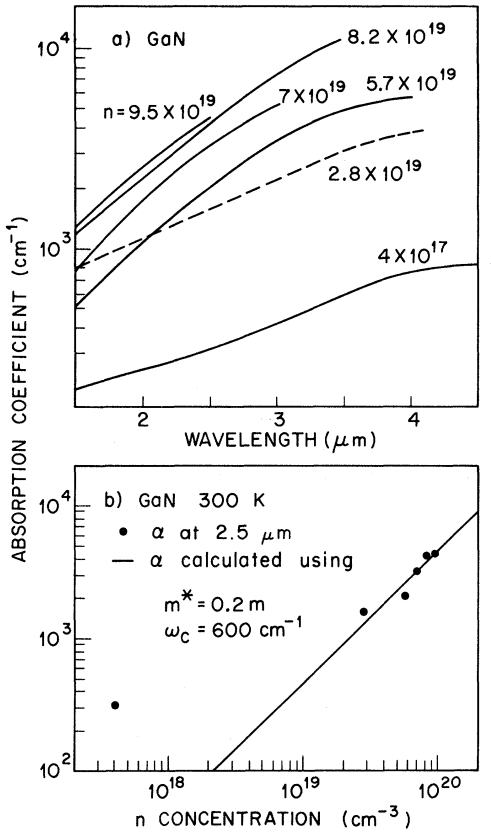

FIG. 8. (a) Absorption coefficient of several GaN samples measured by transmission. The curves are labeled with the electron concentration determined by Hall measurements. (b) Absorption at $\lambda = 2.5$ μm taken from the spectra above plotted against carrier concentration. The solid curve is calculated assuming the values of m^* and ω_c shown.

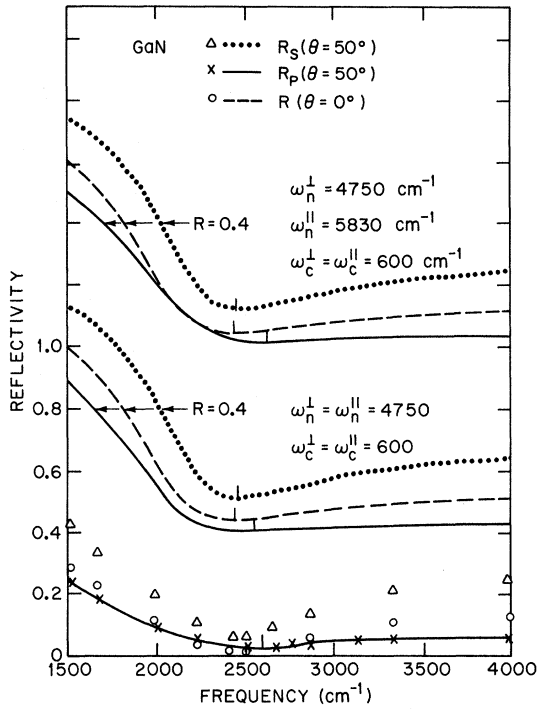

FIG. 9. R_s and R_p reflectivity of GaN at non-normal incidence to determine anisotropy of free-carrier dispersion. The points give the experimental data. The curves are theoretical calculations for isotropic carriers and one case of anisotropic carriers. They have been displaced vertically for clarity. The solid curve drawn through the experimental points is for convenience only. Small vertical lines mark the minimum point on each curve.

Unlike the situation mentioned above for the reflectivity minimum, α depends directly on ω_c as well as on n/m^* through the ω_n^2 factor. Figure 8(b) shows the absorption at 4000 cm^{-1} plotted against concentration determined by the Hall measurements. Again there is a good correlation. Several reflectivity fits have shown that $\omega_c \simeq 600$ cm^{-1}. Adopting this value of ω_c and Eq. (11) for m^* we have plotted Eq. (12) with no adjustable parameters as a solid curve in Fig. 8(b). Except for the lowest concentration point the fit is good giving an independent confirmation of the value $m^* = 0.2$ m. The results of Fig. 8(a) appear qualitatively very similar to those given recently by Cunningham *et al.*,[17] although the absorption coefficients measured here lie considerably above the data of Ref. 17.

All of the above measurements used to determine m^* were performed at near normal incidence. These measurements determine m^* for the ϵ^{xx} dielectric tensor component, i.e., the mass for carrier motion in the wurtzite x-y plane. As discussed in Sec. IV B non-normal incidence may be used to measure ϵ^{zz}. We have made one such measurement on a sample with 5.8×10^{19} electrons/cm^3. Surface roughness is more critical in this measurement where the reflectivity edge is near 4 μm. Figure 9 shows the measured spectrum. From the normal-incidence data we can establish that $\omega_n^\perp = 4750$ cm^{-1} for this sample. The measured R_p at $\theta = 50°$ shows a shift of R_p (minimum) of about 100 cm^{-1} to higher frequencies. Such a shift is expected for isotropic behavior as the theoretical curves show. Unfortunately there is a poor fit to the isotropic theory in detail, since the measured R_p ($\theta = 50°$) crosses the R ($\theta = 0°$) curve. This situation should happen only if $\omega_n^\parallel$ is greater than $\omega_n^\perp$. We show such a case at the top of the figure for $\omega_n^{\parallel 2}$ 50% greater than $\omega_n^{\perp 2}$.

Intercomparison of several theoretical curves and allowance for the experimental uncertainty leads to the conclusion that ω_n^2 is isotropic to better than 30%. Table III lists our conclusions on both m^* and ω_c from these considerations.

ACKNOWLEDGMENTS

The authors are indebted to C. Adams for the ellipsometry result quoted in this paper. Technical assistance by J. A. Ditzenberger for the optical measurements, R. B. Zetterstrom for crystal growth, and S. Bortas for crystal polishing are gratefully acknowledged.

[1]R. Dingle, D. D. Sell, S. E. Stokowski, and M. Ilegems, Phys. Rev. B **4**, 1211 (1971).
[2]R. Dingle, K. L. Shaklee, R. F. Leheny, and R. B. Zetterstrom, Appl. Phys. Lett. **19**, 5 (1971).
[3]J. I. Pankove, E. A. Miller, and J. E. Berkeyheiser, RCA Rev. (Radio Corp. Am.) **32**, 383 (1971).
[4]D. D. Manchon, A. S. Barker, Jr., P. J. Dean, and R. B. Zetterstrom, Solid State Commun. **8**, 1227 (1970).
[5]M. Ilegems, J. Cryst. Growth **13/14**, 360 (1972).
[6]M. Ilegems and H. C. Montgomery, J. Phys. Chem. Solids (to be published).
[7]W. G. Spitzer and D. A. Kleinman, Phys. Rev. **121**, 1324 (1961).
[8]A. S. Barker, Jr., A. A. Ballman, and J. A. Ditzenberger, Phys. Rev. B **2**, 4233 (1970).
[9]E. Ejder, Phys. Status Solidi **6a**, 445 (1971).
[10]M. Ilegems, R. Dingle, and R. A. Logan, J. Appl. Phys. **43**, 3797 (1972).
[11]See *Lattice Dynamics*, edited by R. F. Wallis (Pergamon, Oxford, 1965), Sec. Cl.
[12]C. Kittel, *Quantum Theory of Solids* (Wiley, New York, 1963).
[13]While the tensor notation in Eqs. (4)–(6) is correct and general for any crystal of orthorhombic or higher symmetry with the plane of incidence parallel to the x-z plane (Fig. 1), we follow the usual custom for uniaxial crystals and use the notation $\epsilon^\perp \equiv \epsilon^{xx} = \epsilon^{yy}$ and $\epsilon^\parallel \equiv \epsilon^{zz}$.
[14]C. A. Arguello, D. L. Rousseau, and S. P. S. Porto, Phys. Rev. **181**, 1351 (1969).
[15]H. W. Verleur and A. S. Barker, Jr., Phys. Rev. **155**, 750 (1967).
[16]R. Dingle and M. Ilegems, Solid State Commun. **9**, 175

(1971). Using the values $m^*=0.20m$ and $\epsilon_0=9.5$ one predicts a value of 30 meV for the effective mass binding energy, in agreement with the observed thermal activation energy for shallow donors.

[17]R. D. Cunningham, R. W. Brander, N. D. Knee, and D. K. Wickenden, J. Lumin. **5**, 21 (1972).

PHYSICAL REVIEW B VOLUME 7, NUMBER 2 15 JANUARY 1973

Electronic Structure of Disordered Systems. II. One-Dimensional Arrays, Bound Bands*

J. C. Wang and K. S. Dy
Department of Physics, University of North Carolina, Chapel Hill, North Carolina 27514
and
Shi-Yu Wu
Department of Physics, University of Louisville, Louisville, Kentucky 40208
(Received 31 July 1972)

The structure of the bound band of a one-dimensional disordered array of attractive δ-function potentials was calculated using the method of Wu and Dy.

I. INTRODUCTION

In a previous paper[1] (referred to as I), we presented a method for calculating the electronic density of states in disordered systems. We showed that the method can be easily generalized to systems with structural disorder. Here we apply the method to calculate the density of bound states for an electron in a one-dimensional disordered array of attractive δ-function potentials of a given strength. Other methods of solving this particular problem exist.[2-6] Our purpose here is to illustrate how the method presented in I works and to provide insight for the application of the method to three-dimensional problems.

Although the one-dimensional disordered array is not a topological disordered system, we have not taken the advantage of the sequential numbering of the atomic sites to reduce the problem into an ordered one. We also do not use the closely connected method of relating the energy eigenvalue to the number of nodes in the wave function. Thus our method of calculation can be readily extended to two and three dimensions. However, as a basis for comparison, we also calculate the exact density of states by the node-counting method of Lax and Phillips.[2]

We shall consider only arrays having short-range order, as defined by Gubanov,[7] in the following way: The distance between each pair of neighboring atoms is taken to be $a(1+\epsilon\gamma)$, where a is the average interatomic spacing L/N, with L being the length of the chain and N the number of atoms in the chain. The factor ϵ is a positive number less than 1 (called the short-range order parameter) and γ is a random number having a Gaussian distribution with $\langle\gamma\rangle=0$, $\langle\gamma^2\rangle=1$. Makinson and Roberts[3] have computed the density of states of one-dimensional arrays of δ-function potentials with ϵ ranging from 0 to 0.1. The results presented, however, are for the positive-energy region only. In this work we have calculated the energy-level distribution in the negative-energy region for the same range of ϵ.

II. METHOD OF CALCULATION

We use the Green's-function formulation presented in I to calculate the density of states. The Hamiltonian we consider is given by

$$H=\frac{p^2}{2m}-\sum_l V_0\delta(x-l)\,, \tag{2.1}$$

where V_0 is a positive number which defines the strength of the potential and l denotes the atomic sites. The tight-binding wave function is taken to be the eigenstate

$$\phi(x-l)=\left(\frac{mV_0}{\hbar^2}\right)^{1/2}\exp\left(-\frac{mV_0}{\hbar^2}\,|x-l|\right) \tag{2.2}$$

of

$$h=\frac{p^2}{2m}-V_0\delta(x-l)\,, \tag{2.3}$$

with eigenvalue

$$w=-\frac{mV_0^2}{2\hbar^2}\,. \tag{2.4}$$

For simplicity we set w equal to -1. Using (2.2) one can easily compute the matrix elements of the total Hamiltonian

$$H_{ll'}=w\delta_{ll'}+2w\sum_{l''\neq l}\exp\left(-\frac{mV_0}{\hbar^2}\times(|l''-l|+|l''-l'|)\right). \tag{2.5}$$